Underlying event and correlation results from CMS

W.Y.Wang[1,a]

[1]*Physics Department, National University of Singapore, Singapore*
On behalf of the CMS Collaboration

Abstract. The underlying event activity in pp collisions is measured using events with a leading charged-particle jet. The activity is measured independently in the two halves of the region transverse to the leading object, containing the maximum and minimum activities. Complementary to the underlying event analysis, the observation of long-range two-particle correlations in high energy heavy ion collisions opens opportunities to explore QCD in quark gluon plasma, the hot dense matter created in heavy ion collisions. The observation of similar correlation structures in high multiplicity pp collisions suggests novel QCD effects. We present selected results of the underlying event activity and particle correlations in various collision systems.

1 Introduction

The study of underlying events and particle correlations provide valuable insights into the nature of particle production in Quantum Chromodynamics (QCD). The underlying event (UE) is a measure of the activity mainly coming from soft and semi-hard processes that are not describable by perturbative QCD (pQCD), and its behaviour can be explained by phenomenological models consisting of multi-partonic collisions within a collision region of extended size. Particle correlation studies quantify the two- or multi-particle correlation yields and is sensitive to the initial collision and partonic production geometry.

In heavy ion collisions, two-particle angular correlations provide evidence for the presence of the quark gluon plasma (QGP) [1], a hot and dense fluid formed by the asymptotically free quarks and gluons (partons) of an energetic collision. Of particular interest are the features in the $\Delta\eta$-$\Delta\phi$ correlation which reveal information on the physics of particle production. Particle correlations due to the production of jets are strongly reflected in the two-dimensional correlation yield as a peak at $(\Delta\eta, \Delta\phi) = (0, 0)$. Momentum conservation in di-jet events is manifested as a corresponding away side peak centred around $(0, \pi)$ with a larger spread in $\Delta\eta$ due to the longitudinal momentum distribution of partons in the colliding nucleons and hydrodynamical effects. The novel long range near side structure, a ridge structure in the $\Delta\phi \approx 0$ side of extended reach in $\Delta\eta$, is believed to be a consequence of the collective expansion of a strongly interacting medium with fluctuations in the initial energy density of the particle production region [2–7].

Similar long range near side ridge structures were also observed for the first time in high multiplicity events for pp collisions at $\sqrt{s} = 7$ TeV [8] and pPb collisions at $\sqrt{s} = 5.02$ TeV [9]. On top of

---

[a]e-mail: w.y.wang@u.nus.edu

hydrodynamical models [10–14], various other production mechanisms have been proposed to explain this phenomenon. These include colour connections in the longitudinal direction [15–18], interaction of the medium with jets [19], colour glass condensates [20–22], and multi-parton interactions (MPI) [23, 24].

Although it remains to be seen whether MPI or other particle production mechanisms are at play in the description of the ridge in pp collisions, MPI have already been widely implemented in various Monte Carlo (MC) generators to explain the UE activity. The UE activity is defined as the final-state activity on top of the ones coming from the most hardest partonic scattering of a collision. Most of the activity is dominated by soft radiation beyond pQCD regimes and is poorly understood. The understanding of the UE activity then comes from the implementation of the phenomenological modeling of MPI in MC generators. In the MC generators, the MPI are implemented either as the multiple scattering of partons with a Poissonian number of interactions that has an average that depends on the impact parameter of the hadronic collision [25, 26] or by a Gribov-Regge approach to the multiple scattering of Pomerons [27].

In the MPI model, hadron production in a proton-proton (pp) collision is understood to originate from multiple scatterings of the partonic constituents in a collision region of extended spatial dimensions. The activity coming from MPI cannot be uniquely separated from the radiation coming from the hardest partonic scattering. However, experimentally "clean" observables that are relatively uncontaminated by the radiation from the hardest partonic scattering can be defined as the UE activity. The UE activity is then comprised of hadrons coming from MPI, initial- and final-state radiation (ISR, FSR), and proton remnants concentrated along the beam direction.

Recent results on the UE activity at $\sqrt{s}$ = 2.76 TeV are shown for pp collisions and compared to previous measurements at 0.9 and 7 TeV. Two-particle correlations at $\sqrt{s}$ = 7 and 13 TeV are also shown.

2 Underlying event

The UE activity at $\sqrt{s}$ = 2.76 TeV is measured in events containing a leading charged-particle jet [28] as a probe for a hard interaction. The average multiplicity ($\langle N_{chg} \rangle$) and scalar transverse momentum sum ($\langle \Sigma p_T \rangle$) / average energy densities of charged-particles (per unit η and $\Delta\phi$ of the phase space) in the region orthogonal to the azimuthal direction ($60° < |\Delta\phi| < 120°$) of the leading charged-particle jet are then referred to as the UE activities in the transverse region. This definition reduces radiation contamination coming from the hard interaction. To further isolate effects coming from initial- and final-state radiation, the UE densities are separated into transMAX and transMIN densities, where transMAX/transMIN is defined as the half of the transverse region which contains higher/lower activity on an event-by-event basis for each observable.

Leading charged-particle jets are required to have $|\eta| < 2$ and $p_T^{jet} > 1$ GeV. Additionally, only events with a single reconstructed vertex are considered. The charged-particles used for the UE densities are within $|\eta| < 2$ and $p_T > 0.5$ where detector efficiency is high. Observables are fully corrected for detector effects and selection efficiencies. Further details on event selection, particle/track selection, and correction methodology are outlined in Ref. [28].

By studying the transverse, transMIN, and transMAX UE activities as a function of p_T^{jet}, various interesting properties emerge. The transverse densities shown in figure 1 show typical features of the UE activity, with a fast rise in activity followed by a much slower rise for $p_T^{jet} > 8$ GeV. This "saturation" of the activity is more pronounced in particle densities than energy densities and in transMIN compared to transMAX/transverse densities. Further analysis can be done by defining transDIF densities as the difference between transMAX and transMIN densities, which shows a faster rise in the "saturation" region compared to transverse, transMAX, and transMIN densities.
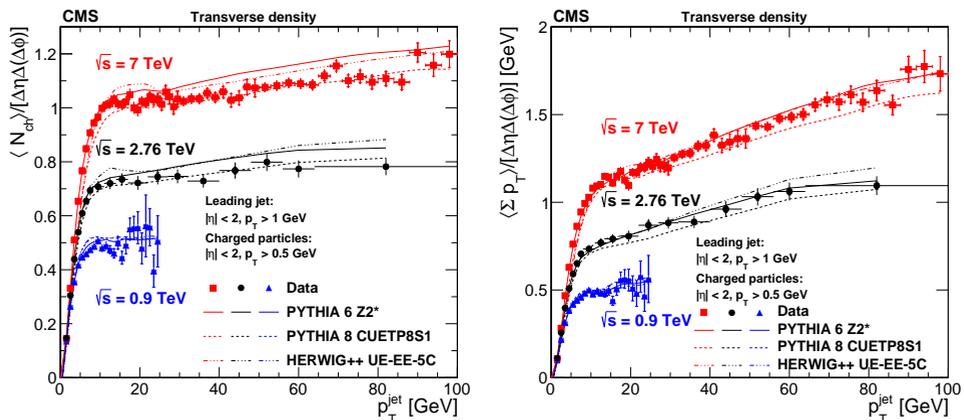
Figure 1. Average transDIF (left) particle and (right) energy densities as a function of p_T^{jet} across 0.9, 2.76, and 7 TeV [29, 30]. The data (symbols) are compared to various MC simulations (curves). The inner error bars correspond to the statistical uncertainties, and the outer error bars represent the statistical and systematic uncertainties added in quadrature.

These characteristics of the UE densities are interpreted in MC generator models as due to the interplay between MPI and the event topology (e.g. jet topology) from hard interactions. The rapid rise in UE densities below ~ 8 GeV is attributed to an increase in MPI with the hard scale of the interaction producing the leading jet. Saturation of the UE activity sets in for events with very hard parton-parton scatterings, which are correlated to nearly maximal overlap of the colliding protons. In such situations where the impact parameter is small, the MPI activity saturates [25, 26]. In two-jet events, the event topology is largely symmetrical about the leading jet axis. However the sub-leading contribution to the inclusive jet cross-section comes from three-jet production, in which case the jet topology of such events would be asymmetrical about the leading jet axis and introduce large fluctuations which can be separated by the definition of transMAX and transMIN densities. TransMAX densities would capture radiation coming from the third jet, while transMIN densities are largely sensitive to the MPI activity which is expected to be uniformly distributed in the azimuthal axis. By definition, transDIF activities are then sensitive to initial- and final-state radiation.

The measured densities are compared to MC simulations from PYTHIA 6 Z2* and CUETP6S1 tunes, PYTHIA 8 4C and CUETP8S1 tunes, as well as HERWIG++ UE-EE-5C tune. The comparisons show reasonable agreement, with the worst performing prediction having up to 15% discrepancy. In general, more recent tunes (CUETP6S1 and CUETP8S1) with parameters optimised by comparison to previous CMS UE data do better in comparison to older tunes. These tunes have up to 10% discrepancy. The total uncertainty of the measured data goes up to 6%. The different MC generators differ mostly in the hadronisation mechanism and the tunes differ by the values of the parameters that control the behaviour of MPI. These are summarised in [28].

The energy dependence of the UE activity across 0.9, 2.76, and 7 TeV is summarised in figure 1. A strong dependence of the UE activity with centre-of-mass energy is seen in the data and also reflected by the various MC simulations.
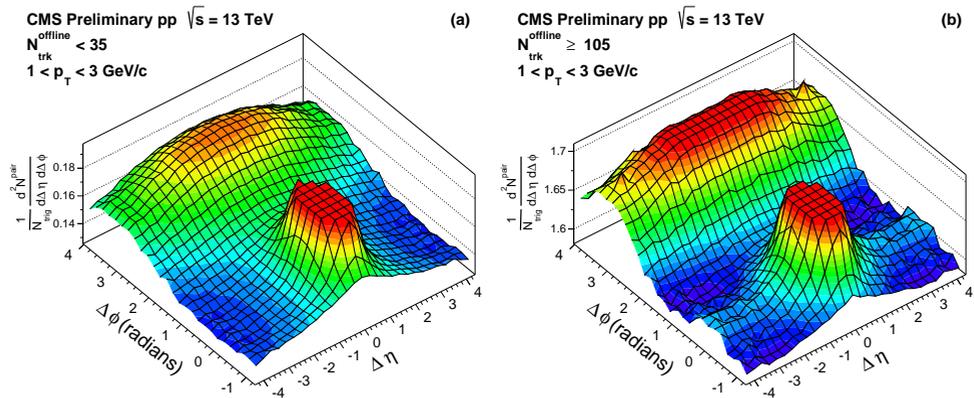
Figure 2. The 2D two-particle correlation functions for (left) low-multiplicity and (right) high-multiplicity events at 13 TeV. The sharp jet peaks are truncated for better illustrations of the long-range correlation.

3 Two-particle correlations

Two-particle correlations are measured at $\sqrt{s} = 13$ TeV [31] using events that contain at least 1 vertex within 15 cm of the nominal interaction point and within 0.15 cm of the beam axis in the transverse plane. With an average of 1.3 pp interactions per bunch crossing, a substantial fraction of events contain PU vertices. To reduce the impact of PU, a PU rejection method [31] is applied. Charged-particles within $|\eta| < 2.4$ and with $p_T > 0.1$ GeV are selected for the analysis. These are selected with respect to the highest-multiplicity vertex in the event. Additional details on event and track selection are in [31].

Events are grouped into multiplicity classes of [2, 35), [35, 80), [80, 105), and [105, 135), and [135, ∞). In each multiplicity class, the particles are also grouped into various p_T intevals. Each particle ("trigger") in a given p_T range is matched with every other remaining particle ("associated") in the same p_T range for which the per-trigger-particle associated yield is defined as

$$\frac{1}{N_{trig}} \frac{d^2 N^{pair}}{d\Delta\eta d\Delta\phi} = B(0,0) \times \frac{S(\Delta\eta, \Delta\phi)}{B(\Delta\eta, \Delta\phi)}, \tag{1}$$

where $\Delta\eta$ and $\Delta\phi$ are the relative differences in η and ϕ of the matched particles (pairs), N_{trig} is the number of trigger particles, and N^{pair} denotes the number of pairs. The signal and background distributions $S(\Delta\eta, \Delta\phi)$ and $B(\Delta\eta, \Delta\phi)$ are defined as

$$S(\Delta\eta, \Delta\phi) = \frac{1}{N_{trig}} \frac{d^2 N^{same}}{d\Delta\eta d\Delta\phi} \tag{2}$$

$$B(\Delta\eta, \Delta\phi) = \frac{1}{N_{trig}} \frac{d^2 N^{mix}}{d\Delta\eta d\Delta\phi}, \tag{3}$$

where N^{same} and N^{mix} refers to the number of pairs in the same event and different events (accounting for random combinatorial background and pair acceptance effects) respectively. Figure 2 shows the 2-dimensional (2D) correlation functions for events with low (less than 35) and high (at least 105)
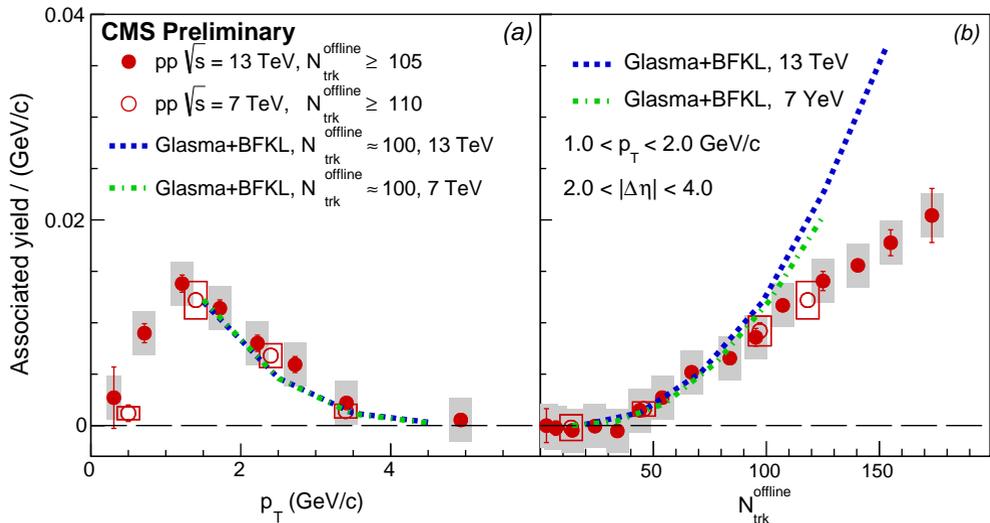
Figure 3. Associated yield as a function of (left) p_T and (right) $N_{trk}^{offline}$ for the near-side of the correlation function averaged over $2 < |\Delta\eta| < 4$ and integrated over the region $|\Delta\phi| < \Delta\phi_{ZYAM}$ for pp data at $\sqrt{s} = 13$ TeV (filled circles) and 7 TeV (open circles). Error bars correspond to statistical uncertainties, while the shaded areas and boxes denote the systematic uncertainties.

track multiplicity ($N_{trk}^{offline}$). The ridge structure described in section 1 emerges for high multiplicity events. This is not predicted in the PYTHIA MC generator.

In order to quantify the long-range, near-side correlations, one-dimensional (1D) distributions in $\Delta\phi$ are derived by averaging the signal and background 2D distributions over $2 < |\Delta\eta| < 4$ and the correlated portion of the associated yield is estimated using an implementation of the zero-yield-at-minimum (ZYAM) procedure that substracts the minimum value of a fit function from the 1D correlation such that the minimum of the correlation function is zero. The location of the minimum is denoted as $\Delta\phi_{ZYAM}$. Figure 3 shows the integrated yield over $\Delta\phi$ and as a function of p_T for events with $N_{trk}^{offline} \geq 105$ at $\sqrt{s} = 13$ TeV and $N_{trk}^{offline} \geq 110$ at $\sqrt{s} = 7$ TeV, as well as a function of $N_{trk}^{offline}$ for a selection of $1 < p_T < 2$ GeV on both particles in the pair. The yield peaks at around $p_T = 1$ GeV and then decreases with increasing p_T. No centre-of-mass energy dependence is visible. For low multiplicity events, the yield is consistent with zero up to about $N_{trk}^{offline} = 40$ and an approximate linear rise above that. Comparison with gluon saturation models show a qualitative agreement in the yields as well as its centre-of-mass energy dependence. However the predictions deviate from the data points in high multiplicity events. Comparison of the integrated yields across different collision systems show a similar trend with yields from pp collisions where the yield starts to rise for $N_{trk}^{offline} \geq 40$. While there is no clear centre-of-mass dependence, a strong collision system size dependence is seen in figure 4.

4 Summary

The underlying event activity is measured with a leading charged-particle jet and quantified in various transverse activities. The measurement lends credence to the MPI model and comparison of the
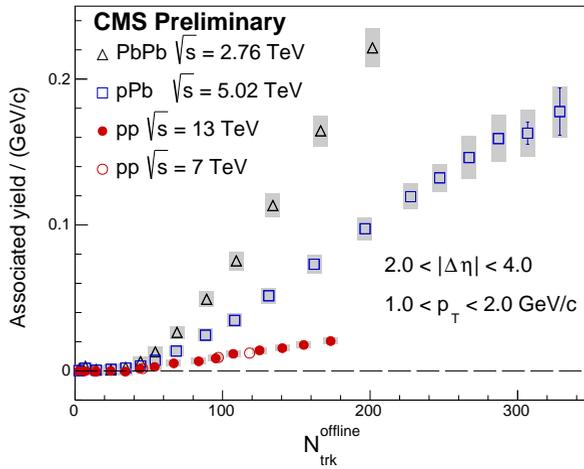
Figure 4. Integrated associated yield as a function of $N_{trk}^{offline}$ for the near-side of the correlation function for *pp* collisions at $\sqrt{s}$ = 7 and 13 TeV, *pPb* collisions at $\sqrt{s_{NN}}$ = 5.02 TeV, and *PbPb* collisions at $\sqrt{s_{NN}}$ = 2.76 TeV. Presentation of errors are the same as figure 3.

data with various MC model predictions at $\sqrt{s}$ = 0.9, 2.76, and 7 TeV allows for the improvement of the MC model tuning and predictions. Results of two-particle correlations in *pp* collisions at $\sqrt{s}$ = 13 TeV are shown and the long-range near-side yields are compared to results at $\sqrt{s}$ = 7 TeV and shown to be qualitatively the same. Comparison of the yields with different collision systems indicate a strong system size dependence. The observation of such correlations in *pp* collisions has seen various novel mechanisms being proposed to explain the phenomenon. Although it remains unclear which mechanisms are at play, gluon saturation models are shown to be able to qualitatively describe the yields at low multiplicity regimes.

Acknowledgements

References

[1] B. Alver et al., Phys. Rev. C **81**, 024904 (2010)
[2] B. Alver, G. Roland, Phys. Rev. C **81**, 054905 (2010)
[3] B. Alver et al., Phys. Rev. C **82**, 034913 (2010)
[4] B. Schenke, S. Jeon, C. Gale, Phys. Rev. Lett. **106**, 042301 (2011)
[5] H. Petersen et al., Phys. Rev. C **82**, 041901 (2010)
[6] J. Xu, C.M. Ko, Phys. Rev. C **83**, 021903 (2011)
[7] D. Teaney, L. Yan, Phys. Rev. C **83**, 064904 (2011)
[8] V. Khachatryan et al., Journal of High Energy Physics **2010**, 91 (2010)
[9] S. Chatrchyan et al., Physics Letters B **718**, 795 (2013)

[10] E. Avsar et al., Physics Letters B **702**, 394 (2011)

[11] K. Werner, I. Karpenko, T. Pierog, Phys. Rev. Lett. **106**, 122004 (2011)

[12] E. Avsar, Y. Hatta, C. Flensburg, J.Y. Ollitrault, T. Ueda, Journal of Physics G: Nuclear and Particle Physics **38**, 124053 (2011)

[13] P. Bożek, Phys. Rev. C **85**, 014911 (2012)

[14] P. Bożek, W. Broniowski, Physics Letters B **718**, 1557 (2013)

[15] Arbuzov, B.A., Boos, E.E., Savrin, V.I., Eur. Phys. J. C **71**, 1730 (2011)

[16] K. Dusling, R. Venugopalan, Phys. Rev. D **87**, 051502 (2013)

[17] K. Dusling, R. Venugopalan, Phys. Rev. D **87**, 054014 (2013)

[18] Y.V. Kovchegov, D.E. Wertepny, Nuclear Physics A **906**, 50 (2013)

[19] C.Y. Wong, Phys. Rev. C **84**, 024901 (2011)

[20] K. Dusling, R. Venugopalan, Phys. Rev. D **87**, 094034 (2013)

[21] A. Dumitru, K. Dusling, F. Gelis, J. Jalilian-Marian, T. Lappi, R. Venugopalan, Physics Letters B **697**, 21 (2011)

[22] K. Dusling, R. Venugopalan, Phys. Rev. Lett. **108**, 262001 (2012)

[23] M. Strikman, Acta. Phys. Pol. **42**, 2607 (2011)

[24] S. Alderweireldt, P. Van Mechelen (2012), `arXiv:1203.2048`

[25] T. Sjöstrand, M.V. Zijl, Physics Letters B **188**, 149 (1987)

[26] L. Frankfurt, M. Strikman, C. Weiss, Phys. Rev. D **83**, 054012 (2011)

[27] H. J. Drescher and others, Phys. Rept. **350**, 93 (2001), `hep-ph/0007198`

[28] V. Khachatryan et al. (CMS), JHEP **09**, 137 (2015), `1507.07229`

[29] S. Chatrchyan et al. (CMS), JHEP **09**, 109 (2011)

[30] V. Khachatryan et al. (CMS), Eur. Phys. J. C **70**, 555 (2010)

[31] CMS Collaboration (CMS), CMS Physics Analysis Summary CMS-PAS-FSQ-15-002 (2015), `http://cds.cern.ch/record/2056346?ln=en`